Tropical anomalies associated with the interannual variability of the cross-equatorial flows over the Maritime Continent in boreal summer

Article

Accepted Version

Tropical anomalies associated with the interannual variability of the cross-equatorial flows over the Maritime Continent in boreal summer

Xiaoxuan Zhao[1], Riyu Lu[2, 3*], Buwen Dong[4], Xiaowei Hong[5], Junqi Liu[2, 3], Jianqi Sun[1, 3]

1. *Nansen-Zhu International Research Center, Institute of Atmospheric Physics, Chinese Academy of Sciences, Beijing 100029, China*
2. *State Key Laboratory of Numerical Modeling for Atmospheric Sciences and Geophysical Fluid Dynamics, Institute of Atmospheric Physics, Chinese Academy of Sciences, Beijing 100029, China*
3. *College of Earth and Planetary Sciences, University of Chinese Academy of Sciences, Beijing 100049, China*
4. *Department of Meteorology, National Centre for Atmospheric Science, University of Reading, Reading, UK*
5. *Climate Change Research Center, Institute of Atmospheric Physics, Chinese Academy of Sciences, Beijing 100029, China.*

[*]*Corresponding author*: Riyu Lu

E–mail address: lr@mail.iap.ac.cn

ABSTRACT

In this study, we investigate circulation, convection, and sea surface temperature (SST) anomalies associated with interannual variability of the cross-equatorial flows (CEF) intensity over the Maritime Continent (MC) in boreal summer. Observational diagnostics show that strengthened CEF is associated with large-scale circulation anomalies featured by weakened Walker circulation, upper-level northeasterly anomalies across MC, and lower-level cyclonic anomalies over the tropical Western North Pacific (WNP). Further analyses indicate that strengthened CEF is associated with both La Niña-like SST anomalies in preceding winter and El Niño-like SST anomalies in simultaneous summer. These relationships between CEF and ENSO are established by two convection key regions: enhanced convection over WNP and depressed convection over MC. A linear baroclinic model is applied here to further discuss the causality between circulation and convection. Results suggest that both the WNP heating and MC cooling can induce the strengthened CEF. Moreover, the stability of the relationship between CEF and El Niño-Southern Oscillation (ENSO) is also discussed. Results show that the relationship between CEF and SST anomalies in the simultaneous summer is stable and keeps significant, while that between CEF and SST anomalies in the preceding winter experienced a decadal strengthening around 1997/98 from insignificant to significant. After 1998, the preceding winter ENSO is followed by strong summer SST anomalies in MC and thus significantly affect CEF via modulating local convection. However, this ENSO-summer MC SST relationship is weak before 1997, failing to establish the relationship between the preceding ENSO and CEF.

1 Introduction

In boreal summer, several channels of airflows over tropical areas can be found across the equator from the Southern Hemisphere (SH) to Northern Hemisphere (NH) in the lower troposphere, which are referred to as the cross-equatorial flows (CEFs; Rodwell and Hoskins 1995; Shi et al. 2007; Wang and Yang 2008; Li and Li 2014). Among these, CEFs in the Eastern Hemisphere are well known to play a significant role in the water vapor transport from the Southern Hemisphere to the Asian monsoon regions and modulate the resultant

rainfall (Dao et al. 1962; Findlater 1969; Wang and Li 1982; Lau and Li 1984; Wang and Xue 2003; Li et al. 2018). Meanwhile, CEFs are products of the energy imbalance between SH and NH (Zeng and Li, 2002), and can be used to estimate the location of ITCZ and the strengths of subtropical highs to some extent based on the energetic framework (Schneider et al. 2014; Song et al. 2018a, b).

Among CEFs in the Eastern Hemisphere, CEFs over the Maritime Continent (MC) show the strongest variability on the interannual timescale and are closely related to the climate variability of East Asia (Zhu 2012; Li and Li 2014; Zhao and Lu 2020). Previous studies pointed out that the variation of CEFs over MC can modulate the distribution of summer rainfall over China (Zhu, 2012; Wang and Yang, 2014), and plays a significant role in the extreme rainfall events over the Yangtze and Huai River Basin (Li et al. 2000). Meanwhile, CEFs over MC are regarded as an important factor to the onset of the South China Sea summer monsoon (Gao and Xue, 2006), maintaining of the WNP monsoon trough (Lin and Chou, 2014), and the activities of tropical cyclones (Xu, 2011; Feng et al., 2017). In this study, we focus on the interannual variability of CEF over MC, which is hereafter referred to as CEF for short unless noted otherwise.

As a significant component of the tropical circulation, the interannual variation of CEF was found to be related to large-scale circulation anomalies in the mid-low latitude. Strengthened CEF is associated with the lower-level anomalous westerlies over the tropical Pacific (Tang et al. 2009; Wang and Yang 2014) and anomalous easterlies over the Indian Ocean (Li and Li, 2014). This pattern of circulation anomalies is often regarded as accompanying El Niño-Southern Oscillation (ENSO). Previous studies have confirmed the relationship between CEF interannual variability and ENSO. Zhu (2012) found El Niño-like sea surface temperature (SST) anomalies over MC and the tropical Pacific in the simultaneous summer associated with the strengthening of CEF. Wang and Yang (2014) further discussed the anomalous SST evolutions in the simultaneous and following seasons and showed that the strengthened CEF is associated with the El Niño developing phase. Li and Li (2014) analyzed the SST anomalies associated with the seesaw pattern between the CEF and Somali jet and found that this seesaw relationship coincides with the developing phase of ENSO. Li et al. (2017) confirmed that the variation of CEF is closely related to the simultaneous SST

anomalies in the equatorial central and eastern Pacific, and indicated that a climate model, forced by observed SSTs, can capture well the interannual variation of CEF, suggesting that the SST anomalies play a crucial role in affecting CEF. However, existing studies mainly found the relationship between ENSO and CEF, there is still a lack of understanding on the specific physical process of how ENSO acts on CEF. In this study, we will explain from the perspective of large-scale convection. Considering the strong coupling between circulation and convection in the tropics, we will also provide our comprehension on the causal relationship by using a simple model. Besides, previous studies mainly focus on the relationship between CEF and ENSO in the simultaneous summer or following seasons. As a continuous process, would ENSO in the preceding seasons also matter the variability of CEF? If so, what are the underlying physical mechanisms?

It has been well documented that the ENSO features, including the spatial pattern and temporal evolution of SST anomalies in the tropics, can change on the decadal timescale (e.g. Kao and Yu 2009; Kug et al. 2009; Yeh et al. 2009; Xiang et al. 2012; Yu et al. 2012; Yeh et al. 2015). Accordingly, the interannual relationship between ENSO and climate variability in various regions, including the Indian monsoon region, East Asia, and the western North Pacific, has experienced significant changes (e.g., Kumar et al. 1999; Wu and Wang 2002; Chen et al. 2012; Zhao and Wang 2018; Wu and Wang 2019). Feng et al. (2014) and Song and Zhou (2015) further pointed out that PDO may play a crucial role in the varying relationship by modulating the background circulation and convection over the WNP region. Does the relationship between ENSO and CEF change or not in the past several decades? If yes, what are the physical mechanisms responsible for the decadal change? These questions are also to be dealt with in this study.

CEF is not confined within the lower levels, though the above research on CEF variability mainly focus on individual pressure levels in the lower troposphere. For a better understanding of CEF variability, some studies gradually started to discuss the upper level, especially the vertical structure of the CEF variability in the whole troposphere. Cong et al. (2007) found that strong northerly anomalies at 200 hPa correspond to the strengthened CEF at 850 hPa. Zhao and Lu (2020) further indicated a strong seesaw relationship between the interannual variability of the upper- and lower-level CEF, which acts as the leading mode of

the interannual variability in the meridional winds along the equator. Here, we consider the upper- and lower-level CEF as a coupling and discuss the corresponding horizontal circulation anomalies on both the upper and lower troposphere.

In this study, we investigate the variation of horizontal winds, atmospheric convections, and SSTs in the tropics, associated with the CEF interannual variability. Special attentions are paid to the evolution of ENSO, i.e., the tropical SST anomalies in the preceding seasons, in addition to the simultaneous and following seasons, are considered. More importantly, we attempt to figure out how these SST anomalies affect the CEF by convection activities. To illustrate the causality between circulation and convection, we adopt a simple model that will be introduced in the next section. The robustness of the relationship between the interannual variability of CEF and SST evolution is also examined. The rest of this paper is arranged as follows. Section 2 describes the reanalysis data and simple model used in this study. Section 3 displays the circulation, convection, and SST anomalies associated with the CEF interannual variability. Section 4 shows the possible impacts of convection over key regions of WNP and MC on CEF variability based on observational data and a simple model. Section 5 examines the stability of the relationship between CEF and SST anomalies in the preceding winter and simultaneous summer, and clarifies the possible physical processes. Section 6 devotes the summary and discussion.

2 Data, indices, and model

In this study, monthly mean meridional and zonal winds are derived from ERA5 (Hersbach et al. 2020) with a resolution of 0.5°×0.5°. Monthly mean interpolated outgoing longwave radiation (OLR) data from NOAA (Liebmann and Smith 1996) with a resolution of 2.5°×2.5° and precipitation data from the Global Precipitation Climatology Project (GPCP) Version-2 (Adler et al. 2003) with a resolution of 2.5°×2.5° are used to depict the convection activities. Besides, SST adopted here is the same as that used in ERA5 as boundary conditions for the atmospheric forecast model (Hersbach et al. 2020), with a resolution of 0.5°×0.5°. All the analyses cover 1979–2020 and are performed on the seasonal mean of June-July-August (JJA). We focus on interannual variation and apply a 9-yr Gaussian filter to remove the decadal and long-term changes. The statistical significance of the results is examined through

the Student's *t*-test.

Two indices are defined to depict the interannual variations of CEFs over MC in the high and low levels. The high-level CEF (HCEF) index is defined as the 200 hPa meridional wind anomalies along the equator averaged over 110°–170°E following Zhao and Lu (2020), but multiplied by minus one in this study. As for the low-level CEF (LCEF), considering that the variability of LCEF on 925 hPa over three channels (i.e., 102.5°–110°E, 122.5°–130°E and 147.5°–152.5°E) adjacent or through the MC show strong coherence (Li and Li, 2014), LCEF index is collectively defined by the 925 hPa meridional wind anomalies along the equator averaged over three channels (Zhao and Lu, 2020). These two indices are then normalized by their corresponding standard deviations and are referred to as HCEFI and LCEFI, respectively. Considering that northerlies and southerlies prevail in the upper and lower troposphere, respectively (figures 1a and b), positive values of both HCEFI and LCEFI represent the strengthening of CEF.

In addition to the observational diagnostics, a linear baroclinic model (LBM) is utilized to help understand the causality between circulation and convection by investigating the atmospheric responses to the prescribed heat forcings. This model adopts the sigma (σ) coordinate system with 20 levels in vertical, and the vertical levels around 200 hPa are 298, 233, 179, and 128, and those around 925 hPa are approximately 980, 950, 900, and 830. The responses at these levels are transformed to the pressure level coordinate system, and the levels for outputs around 200 hPa are 250, 200, and 150 hPa and those around 925 hPa are 950 and 900 hPa. Besides, the horizontal resolution adopts T42, i.e., 64×128. More details can be well referred to Watanabe and Kimoto (2000, 2001). For better understanding the role of individual heat forcing, we use a dry version to avoid possible interactions of responses to prescribed heat forcings from different regions. All experiments are performed in the presence of summer mean flow obtained from ERA5 for 1979–2020. Heat forcings are imposed over the key convection regions according to the reanalysis results, more details are shown in section 4b. The linear atmospheric responses are obtained by the average of day 11 to 20.

3 Circulation, convection, and SST anomalies associated with CEF variability

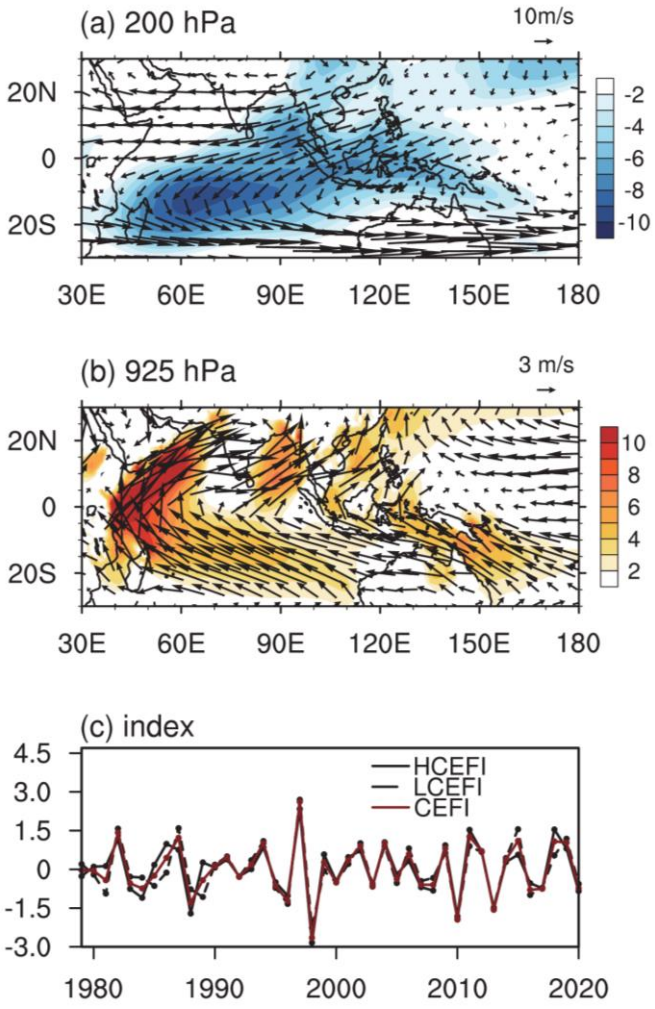

Fig. 1 Climatological wind field (vector, m s^{-1}) at (a) 200 hPa, (b) 925 hPa. The blue (red) shadings represent northerly (southerly) components greater than 2 m s^{-1}. (c) Time series of normalized HCEFI (black solid line), LCEFI (black dashed line), and CEFI (red solid line) in JJA.

The time series of the normalized HCEFI and LCEFI with a 9-yr Gaussian filter applied are shown in Fig. 1c. Concurrent strengthening or weakening between two time series can be found, albeit some discrepancies in the individual years. Considering that the correlation coefficient between HCEFI and LCEFI is as high as 0.85, we define a normalized combined index, named CEFI:

$$CEFI = HCEFI + LCEFI \quad \ldots(3.1)$$

Because both HCEFI and LCEFI have been normalized before they are combined into the CEFI, these two indices contribute equivalently to the CEFI. The CEFI is highly correlated with both HCEFI and LCEFI, with the correlation coefficient being 0.96. The maximum and minimum appear in 1997 and 1998, respectively, reminiscent of the strong El Niño event in

1997/98 winter.

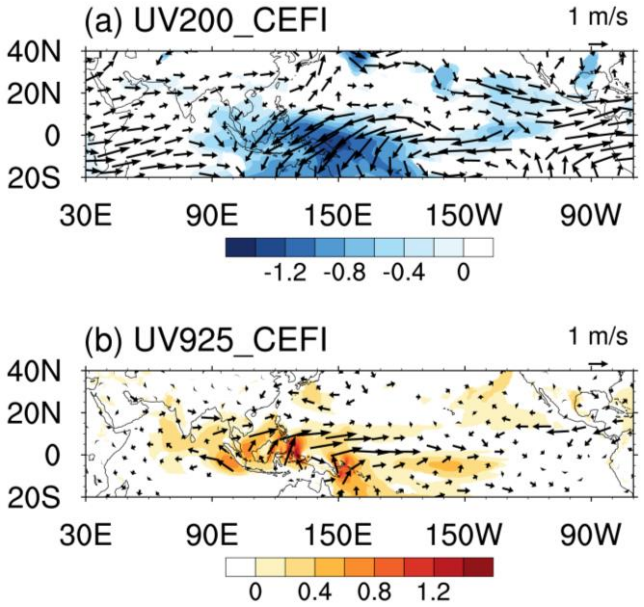

Fig. 2 Regression of the JJA-mean horizontal circulation (vector, m s^{-1}) at (a) 200 hPa, (b) 925 hPa onto the CEFI. The blue (red) shadings represent northerly (southerly) components. Only values passing the 95% confidence level based on the Student's *t*-test are plotted.

As shown in figure 2a, the JJA-mean horizontal wind anomalies associated with the enhanced CEF are strong northeasterlies over MC and the tropical western Pacific at 200 hPa. Accompanied are southerly anomalies distributed in the several channels over MC at 925 hPa (Fig. 2b), consistent with the strong coherence between the HCEFI and LCEFI variations. These meridional wind anomalies are linked with strong and significant zonal wind anomalies in the tropical areas, featured by anomalous westerlies in the Indian Ocean and easterlies in the central and western Pacific in the upper troposphere, and the opposite wind anomalies in the lower troposphere, indicating the weakening of Walker circulation. In addition, an anticyclonic (cyclonic) circulation anomaly can be found in the upper (lower) troposphere over the tropical western North Pacific (WNP).

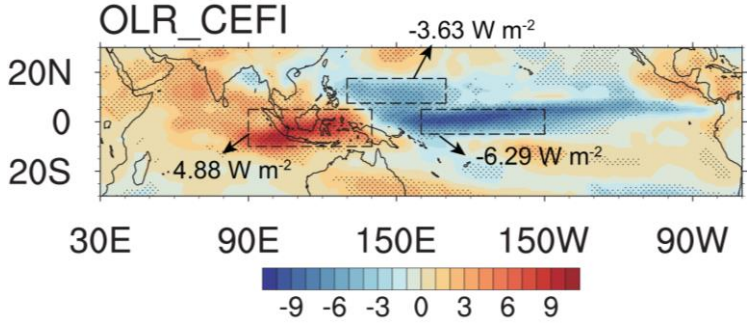

Fig. 3 Regression of the JJA-mean OLR (W m^{-2}) onto the CEFI. The red (blue) shadings

denote the positive (negative) values, and dots represent regions significant at the 95% confidence level based on the Student's *t*-test. Regions framed by rectangles are used to define OLR indices, and the marked values represent the regression coefficient averaged over the rectangle regions. The rectangle regions are (7.5°−17.5°N, 130−170°E), (10°S−5°N, 90°−140°E) and (5°S−5°N, 160°E−150°W) for tropical WNP, MC, and CP, respectively.

Figure 3 shows the spatial distributions of OLR anomalies regressed onto the CEFI. It can be found that the OLR anomalies associated with the strengthening of CEF are featured by suppressed convection over MC and enhanced convection over the tropical Pacific. The average value of CEFI-related OLR anomalies is 4.88 W m^{-2} over MC, and −6.29 W m^{-2} over the central Pacific (CP). In addition, enhanced convection can also be found over the tropical WNP, with the averaged value being −3.63 W m^{-2}.

These convection anomalies are consistent well with the circulation anomalies shown in Fig. 2. The suppressed convection over MC and enhanced convection over the tropical Pacific correspond to the weakened Walker circulation (Figs. 2a and b). Meanwhile, enhanced convection over WNP corresponds to the lower-tropospheric anomalous cyclonic circulation to its northwest (Fig. 2b), which has been well documented by previous studies (e.g., Nitta 1987; Huang and Li 1989; Wang and Fan 1999; Lu 2001; Lu and Dong 2001; Kosaka and Nakamura 2010). In addition to this lower-tropospheric cyclonic anomaly, the anticyclonic anomaly over the WNP in the upper troposphere (Fig. 2a) implies that the circulation responses to heating induced by enhanced convection over the tropical WNP show a baroclinic structure.

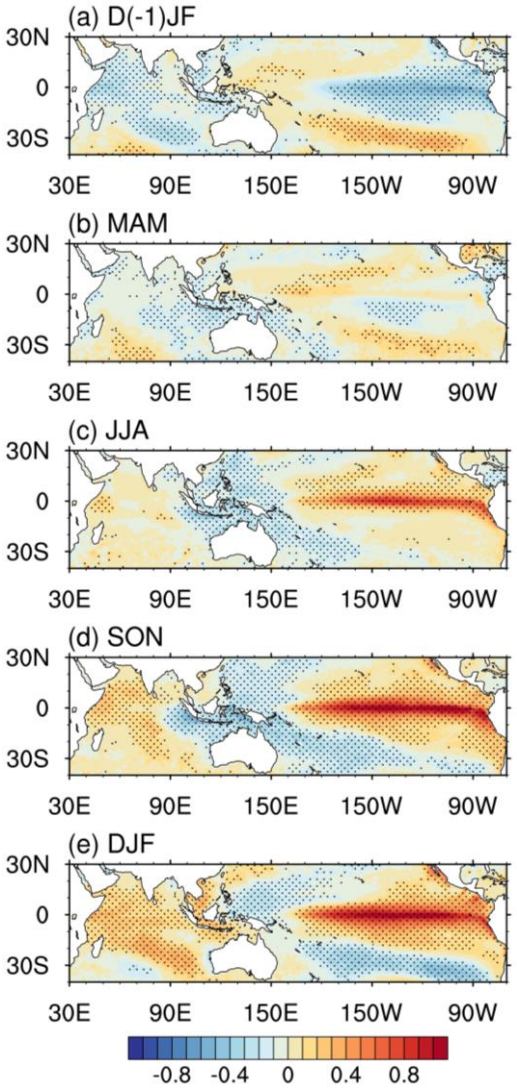

Fig. 4 Regression of the SST (ºC) in (a) D(−1)JF, (b) MAM, (c) JJA, (d) SON and (e) DJF onto the CEFI. The red (blue) shading denotes the positive (negative) values, and dots represent regions significant at the 95% confidence level based on the Student's *t*-test.

Figure 4 shows the SST anomalies from the preceding winter (hereafter referred to as D(−1)JF, i.e., December in the preceding year and January and February in the simultaneous year) to the following winter (DJF, i.e., December in simultaneous year and January and February in subsequent year) regressed onto the JJA CEFI. Cold SST anomalies over the tropical central and eastern Pacific can be found in the preceding seasons along with the strengthening of CEF (Figs. 4a and b). Meanwhile, warm SST anomalies over the western Pacific and cold SST anomalies over the Indian Ocean can also be found. Besides, warm SST anomalies over the tropical central and eastern Pacific emerge simultaneously in JJA and gradually strengthen, reaching a peak in DJF (Figs. 4c–e), accompanied by negative SST

anomalies in the western Pacific and positive anomalies in the Indian Ocean.

Table 1 Correlation coefficients between CEF, convection indices, and Niño 3.4 indices in D(−1)JF and JJA. *(**) represents values significant at the 95% (99.9%) confidence level based on the Student's *t*-test.

	CEFI	WNPI	MCI	D(−1)JF
WNPI	0.64**			
MCI	0.86**	0.33*		
D(−1)JF	−0.38*	−0.63**	−0.17	
JJA	0.81**	0.26	0.81**	−0.12

The correlation coefficients between CEFI and Niño3.4 index in individual seasons are calculated. The correlation coefficient is –0.38 in D(−1)JF, significant at the 95% confidence level, 0.81 in JJA, and 0.78 in DJF (Table 1). These results further confirm that the CEF variability is related to both the preceding negative SST anomalies in the tropical central and eastern Pacific and the simultaneous and following positive anomalies. The relationship between the CEF and simultaneous and following SST anomalies is also mentioned by previous studies (Zhu 2012; Wang and Yang 2014; Li et al. 2017).

It has well known that the El Niño events in the preceding winter lead to the suppressed convection and resultant lower-tropospheric anticyclonic anomaly over WNP (e.g., Wang et al. 2000; Lu and Dong 2001; Xie et al. 2009; Wu et al. 2009; Wu et al. 2010; Song and Zhou, 2014a, b; Xie et al. 2016), and this process explains the WNP part of CEF-regressed circulation and OLR anomalies (Figs. 2 and 3). In addition, the anomalies of Walker circulation and MC convection associated with the developing phase of El Niño events have been well documented (e.g., Philander, 1990; Dai and Wigley 2000; As-syakur et al. 2014), and this association explains the equatorial part of CEF-regressed anomalies. We hypothesize that the tropical convection anomalies may play a crucial role in affecting CEF and thus linking CEF with ENSO. In the following section, this hypothesis will be tested.

4 Impacts of convection over WNP and MC on CEF variability

a. Observational results

The anomalous convections over several key regions closely related to the variability of CEF are selected, i.e., WNP, MC, and CP. To easily characterize the variation of convections over these regions, three OLR indices are defined by averaging OLR anomalies over the specified rectangles as shown in Fig. 3. Considering the fact that enhanced convection over WNP corresponds to stronger CEF (Fig. 3), WNPI is multiplied by minus one. That is, a positive WNPI represents the enhancement of convection, and this modification of the sign of WNPI can facilitate the comparison of results in this section with those shown in the previous sections. Despite the similar situation of convection over the central Pacific, we have not changed the sign of CPI, since as mentioned in the following, convection over the central Pacific may not affect directly the CEF variability. Among these indices, MCI and CPI are highly correlated with each other, with a correlation coefficient being −0.75 through changes in Walker circulation, while WNPI has correlation coefficients of 0.33 with MCI and −0.11 with CPI (Tab. 1).

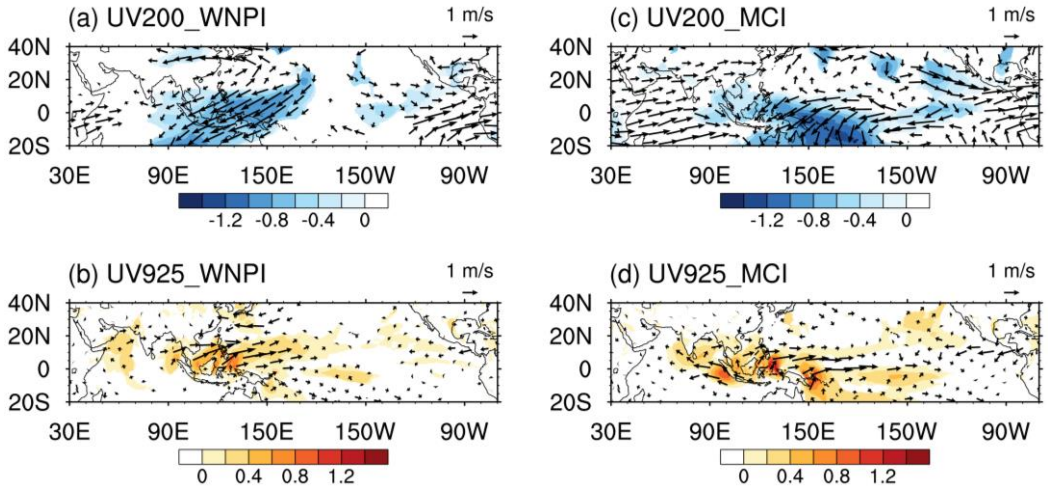

Fig. 5 Regression of the JJA-mean horizontal circulation (vector, m s^{-1}) at (a) 200 hPa, (b) 925 hPa onto the WNPI. (c–d) are the same as (a–b), but for the MCI. The blue (red) shadings represent northerly (southerly) components. Only values passing the 95% confidence level based on the Student's *t*-test are plotted.

Figure 5 shows the horizontal wind anomalies associated with WNPI and MCI, respectively. We also examined the wind anomalies associated with CPI and found that they are very similar to those associated with MCI, which is expectable due to the high correlation

coefficient between these two indices. In addition, in comparison with MCI (0.86), CPI has a relatively lower correlation coefficient with CEFI (−0.75), although it is still high. Therefore, the wind anomalies associated with CPI have not been shown in this paper for brevity. Corresponding to the enhanced WNP convection, strong and significant northeasterly anomalies appear across MC at 200 hPa (Fig. 5a), which is consistent with the CEFI-related wind anomalies (Fig. 2a). These northeasterly anomalies represent an enhancement of the upper-level CEF, and they are connected with an anticyclonic circulation anomaly over the tropical WNP in the upper troposphere. In addition, enhanced convection over WNP corresponds to a cyclonic circulation anomaly in the lower troposphere over the tropical WNP, and a strengthened lower-level CEF is associated with the westerly anomalies at the southern boundary of this cyclonic circulation anomaly (Fig. 5b). Therefore, enhanced convection over WNP corresponds to the strengthening of CEF in both the upper and lower troposphere, which can be re-confirmed by the specific value of meridional wind anomalies averaged over the definition region of HCEFI (LCEFI), which is -0.79 m s^{-1} (0.34 m s^{-1}). Meanwhile, suppressed MC convection corresponds to the upper-tropospheric easterly anomalies in the tropical western and central Pacific and westerly anomalies in the tropical Indian Ocean (Fig. 6c), and roughly opposite-signed zonal wind anomalies in the lower troposphere (Fig. 5d). These zonal wind anomalies connect with the strengthening of both upper- and lower-level CEF, i.e., northerly and southerly anomalies in the upper and lower troposphere, respectively. The specific value of the meridional wind anomalies over the definition region of HCEFI (LCEFI) is -0.77 m s^{-1} (0.6 m s^{-1}).

In summary, the circulation anomalies associated with WNPI and MCI are all characterized by the strengthening of CEF in both the upper and lower troposphere. On the other hand, they also show clear distinctions in the patterns of large-scale circulation anomalies. The stronger CEF along with enhanced WNP convection is respectively associated with the anticyclonic and cyclonic anomaly in the upper and lower troposphere (Figs. 5a and b), but the stronger CEF along with suppressed MC convection is mainly associated with the zonal wind anomalies in the tropical Pacific and the Indian Ocean, i.e., weakened Walker circulations (Figs. 5c and d).

b. Responses of circulation to heat sources

The above observational results demonstrate the close relationship between CEF variability and convection anomalies over the key regions. A simple linear baroclinic model is utilized in this subsection to investigate the responses of circulations to convective heating over the key regions.

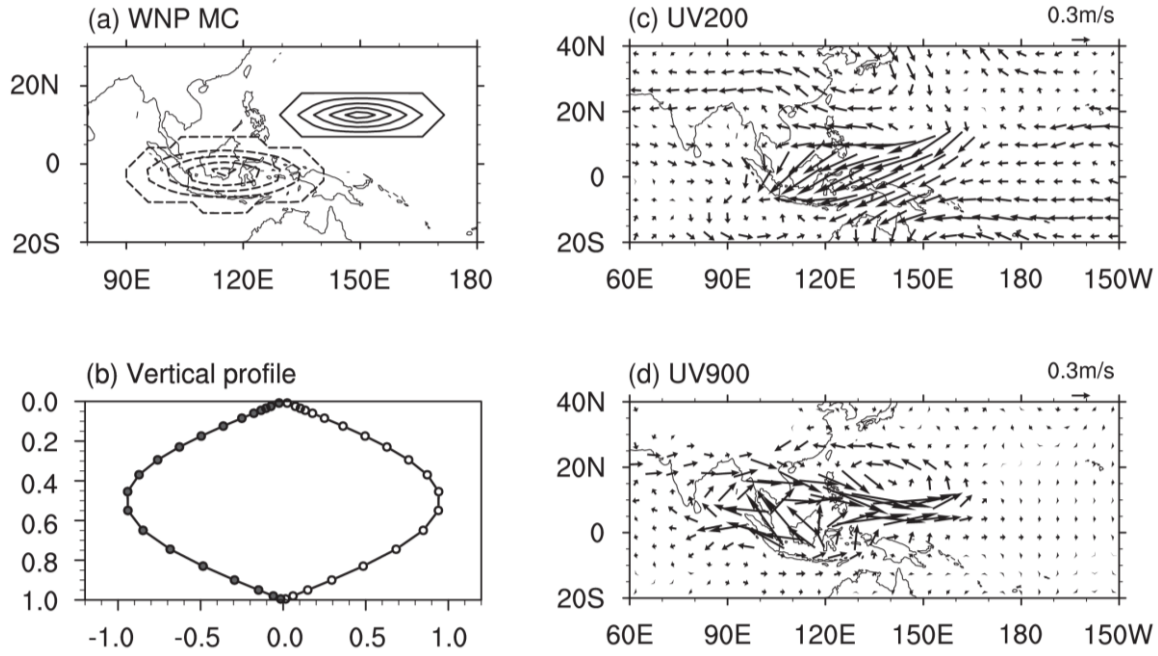

Fig. 6 (a) Horizontal distribution (σ=0.45) and (b) vertical profile of combined heat source over WNP and heat sink imposed over MC. The contour interval of horizontal distribution is 0.2 K day^{-1}. Solid (dashed) lines represent positive (negative) values. The unit of vertical profile is K day^{-1}. (c–d) are the horizontal wind responses at 200 hPa and 900 hPa.

Figure 6a shows the spatial distribution of prescribed heating over WNP and MC, which mimics the convective heating associated with enhanced CEF, that is, a combined heat source over WNP and heat sink over MC. Figure 6b shows the vertical structure of prescribed heating over the heat centers. The maximum of vertical profile is set to be at about 450 hPa (σ=0.45). The intensity of the heat forcings is estimated based on the normalized WNPI- and MCI-regressed precipitation anomalies (not shown), which show a maximum of about 2 mm day^{-1}.

Figures 6c and d show the horizontal circulation in the upper and lower troposphere induced by the prescribed heat forcings. At 200 hPa, strong northeasterlies are induced across MC (Fig. 6c). These northeasterlies indicate the strengthening of upper-level CEF, and the northerly responses averaged over the definition region of HCEFI (110°–170°E along the equator) is 0.28 m s^{-1}. As for the lower level, considering that there is no 925 hPa in LBM, we

use 900 hPa instead (Fig. 6d). Southerly anomalies can be found over the definition channel regions of LCEFI with specific change being 0.36 m s^{-1}. In addition, there is a cyclonic circulation anomaly over the tropical WNP and an anticyclonic circulation anomaly to the southwest of it. These upper- and lower-level circulation responses resemble the wind anomalies associated with the strengthened CEF identified in observations (Fig. 2). The simulated result indicates that the seesaw pattern of convection over WNP and MC can induce the change of CEF in both the upper and lower troposphere.

The specified values of the meridional wind responses in both upper and lower troposphere over the definition region of HCEFI and LCEFI in the simulated results, i.e., 0.28 m s^{-1} and 0.36 m s^{-1}, respectively, are generally smaller than those regressed onto convection over WNP and MC in observations, which range from 0.34 to 0.79 m s^{-1}. The difference between LBM and observational results might result from various factors. For example, the low resolution of LBM (2.8°×2.8°) may lead to the coarse depiction of surface boundary conditions, while the accurate depiction of that is crucial for realistically reproducing the MC precipitation and CEF (Schiemann et al. 2013; Zhuang and Duan 2019). In addition, eddies or synoptic disturbances are strong in summer over WNP and summer-mean eddy activity exhibits strong interannual variability (Fukutomi et al. 2015; Zhou et al. 2018). However, eddies and associated feedbacks from mean-eddy interactions are absent in LBM (Held et al. 1989; Watanabe and Jin 2004). Furthermore, the lack of diabatic heating feedbacks in LBM may also induce differences from observations (Hirota and Takahashi 2012). Therefore, the circulation responses simulated by the LBM should be treated qualitatively, rather than quantitatively, when they are compared with the observed anomalies.

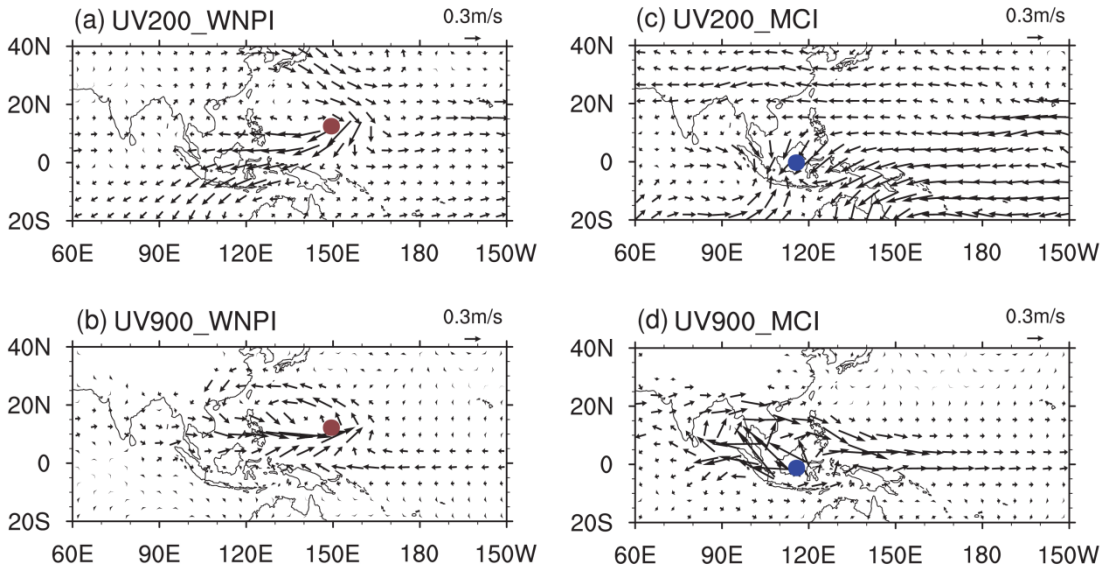

Fig. 7 Horizontal wind responses to the WNP heat source at (a) 200 hPa and (b) 900 hPa. (c–d) are the same as (a–b), but for the MC heat sink. The distribution of heat source (sink) over WNP (MC) is the same as that in Fig. 6, thus only the center is marked by red (blue) dots here.

In the following, heat forcings over WNP and MC are imposed separately to investigate their respective roles. Figures 7a and b show wind responses to the WNP heat source. The heat source over WNP is the same as that in Fig. 6, and its center is marked by the red dot. There are northeasterly responses at 200 hPa across MC (Fig. 7a), indicating the strengthening of the upper-level CEF. At the low level (900 hPa), the wind responses are characterized by the cyclonic circulation over the tropical WNP, and southerly responses appear over MC to the south of this cyclonic circulation (Fig. 7b). These wind responses resemble well the wind anomalies associated with enhanced convection over WNP identified in observations (Figs. 5a and b). The specific value is 0.10 m s^{-1} for the meridional wind responses averaged over the definition region of both HCEFI and LCEFI. Thus, it can be concluded that enhanced convection over WNP induces the strengthening of both upper- and lower-level CEF, as well as stimulating the northeasterlies across MC in the upper troposphere and cyclonic circulation over the tropical WNP in the lower troposphere.

The responses to heat sink over MC are characterized by the easterlies in the tropical Pacific and westerlies in the tropical Indian Ocean in the upper troposphere (Fig. 7c), and by the opposite-signed zonal winds in the lower troposphere (Fig. 7d), indicating a weakened Walker circulation in the tropical Pacific. Associated with these wind responses, northerlies

and southerlies appear over MC in the upper and lower troposphere, indicating the strengthening of both upper- and lower-level CEF. The specific strengthening is 0.18 m s^{-1} for HCEF and 0.26 m s^{-1} for LCEF. These circulation responses highly resemble those associated with the suppressed convection over MC shown in Figs. 5c and d. Thus, suppressed convection over MC can lead to the strengthening of both upper- and lower-level CEF, as well as the weakening of Walker circulation.

We also examined the responses of circulation to prescribed heating over CP and found very weak responses over MC in both the upper and lower troposphere (not shown). The responses of HCEF and LCEF to CP heating are −0.01 and 0.02 m s^{-1}, respectively, and much smaller than those to WNP heating and MC cooling. Therefore, the simulated result confirms that convection over CP does not play a direct role in affecting CEF variability, although it shows a high correlation with CEF (−0.75). The high correlations between CP convection and CEF may be merely a result of the close relationship between CP and MC convection through changes in the Walker circulation.

The hypothesis mentioned in the above section has been so far confirmed that ENSO-like SST anomalies in both preceding winter and simultaneous summer play crucial roles in the interannual variability of CEF via convection activities over WNP and MC. Enhanced WNP convection can induce the strengthening of CEF by northeasterlies across MC in the upper troposphere and cyclonic circulation over WNP in the lower troposphere, and the suppressed MC convection induces the weakened Walker circulation and resultant strengthened CEF.

5 Stability of the relationships between CEF variability and SST anomalies in the preceding winter and simultaneous summer

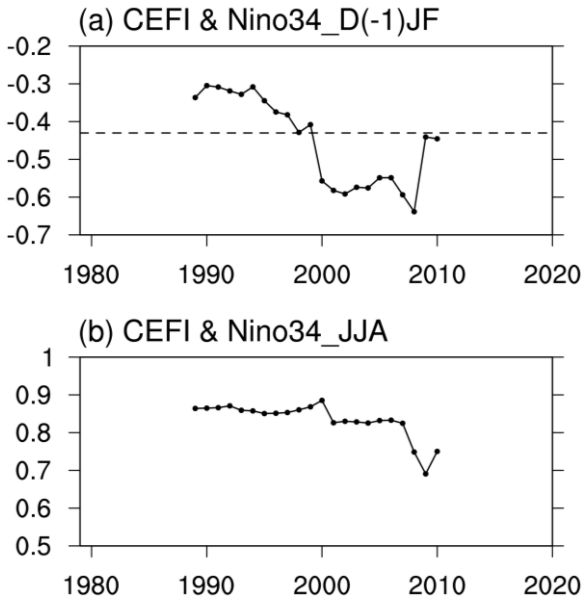

Fig. 8 (a) 21-yr moving correlation between CEFI and (a) Niño 3.4 index in D(–1)JF, (b) Niño 3.4 index in JJA. The dashed line in (a) represents the critical value of the 95% confidence level based on the Student's *t*-test.

Figure 8 shows the 21-yr moving correlation between CEFI and Niño 3.4 index in both preceding winter and simultaneous summer. Relationship between CEF and SST anomalies in D(−1)JF experienced a prominent interdecadal change: The relationship is weak and insignificant before 1999, but strengthens quickly and becomes strong after 2000, with the correlation coefficient being around −0.55, which is significant at the 95% confidence level (figure 8a). Considering that the preceding winter of 1998 witnessed the strongest El Niño event, concurrent with the strongest negative CEF (Fig. 1c), 1998 is supposed to be classified in the latter period. Therefore, the time period is eventually divided as 1979−1997 and 1998−2020. The correlation coefficient between CEFI and the preceding winter Niño 3.4 index is −0.6 in the latter period but is only −0.05 in the former period, confirming the significant strengthening of the relationship. This phenomenon is also prominent in other datasets like JRA55 and NCEP (not shown). In contrast, the relationship between CEFI and the simultaneous Niño 3.4 index is stable (figure 8b), although the correlation coefficient is slightly higher (0.91) in the former period than that in the latter period (0.76).

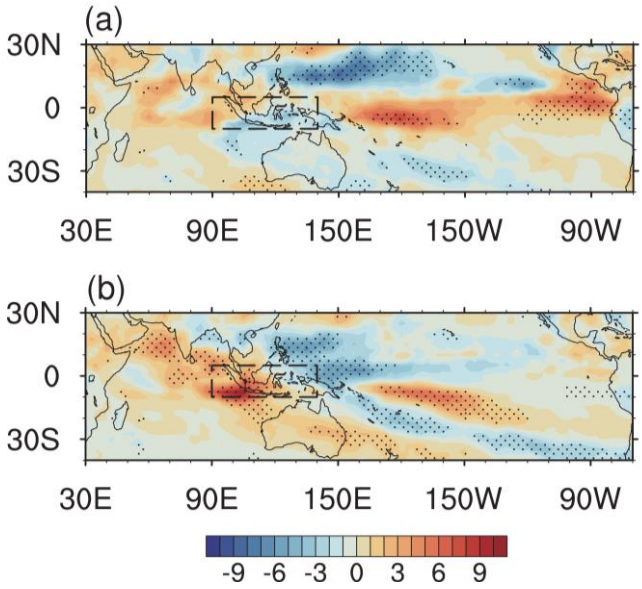

Fig. 9 Regression of the JJA-mean OLR (W m^{-2}) onto the Niño 3.4 index in D(−)JF for the time period of (a) 1979−1997 and (b) 1998−2020. The Niño 3.4 index is multiplied by minus one for comparison. The red (blue) shading denotes the positive (negative) values, and dots represent regions significant at the 95% confidence level based on the Student's *t*-test. Regions framed by rectangles represent the definition region of MCI, which are the same as those in Fig. 3.

In the following, we examine the anomalies associated with the preceding winter Niño3.4 index to investigate the possible reason for the decadal strengthening of its influence on CEFI. Considering the negative relationship between CEFI and the preceding winter Niño3.4 index, the latter index is multiplied by minus one to facilitate the comparison with the CEFI-related anomalies. The JJA-mean OLR anomalies regressed onto D(−)JF −1*Niño3.4 index in two periods are shown in figure 9. Though over many regions the OLR anomalies are distinct between two periods, MC and WNP are focused on in the following, since the convection anomalies over these two regions are closely related to CEF variability. Over MC, OLR anomalies are very weak in the former period but are significantly positive in the latter period. The OLR anomalies averaged over (10°S−5°N, 90°−140°E), i.e., the region used for MCI definition, is −0.33 and 1.85 W m^{-2} in the former and latter periods, respectively. This strengthening relationship can be further verified by the 21-yr moving correlation coefficients between MCI and D(−)JF −1*Niño 3.4 index: They are very weak before the late 1990s, but increase rapidly and become significant afterward (figure 10). The correlation coefficient between MCI and D(−)JF −1*Niño 3.4 index is only −0.05 for 1979−1997 but is 0.35 for

1998−2020. Over WNP, OLR anomalies are negative for both the former and latter periods, albeit with some differences in location and intensity. Therefore, we conclude that negative SST anomalies in the equatorial central and eastern Pacific in the preceding winter lead to stronger CEF via the suppressed convections over MC in the latter period but not in the former period.

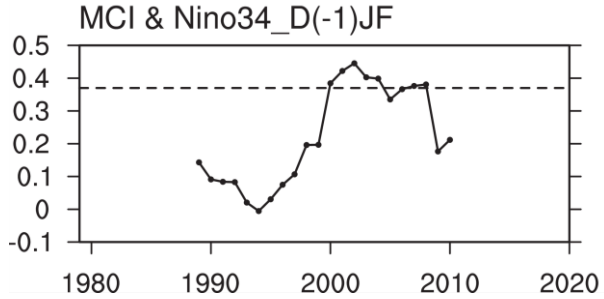

Fig. 10 21-yr moving correlation between MCI and Niño 3.4 index in D(–1)JF. The Niño 3.4 index is multiplied by minus one for comparison. The dashed line represents the critical value of the 90% confidence level based on the Student's *t*-test.

Figure 11 shows the SST anomalies from the preceding winter to summer regressed onto the D(−)JF −1*Niño3.4 index in two periods. SST anomalies in the preceding seasons during the La Niña decaying phase for both periods show similar distributions (Figs. 11a−b, d−e), characterized by negative SST anomalies in the central and eastern Pacific and the Indian Ocean, and positive anomalies over the western Pacific. However, SST anomalies in summer show clear distinctions: The SST anomalies are negative in MC and positive in the equatorial central and eastern Pacific for the latter period but tend to be in opposite signs in the former period. We defined an index as SST anomalies averaged over 10°S−5°N, 90°−140°E, i.e., the region used for MCI definition, and found that the correlation coefficient between this index and the D(−)JF −1*Niño 3.4 index is only −0.12 for the former period, but in the latter period is −0.7, which is significant at the 99.9% confidence level. The pattern of SST anomalies for the latter period is similar to that related to CEFI (Fig. 4c), although the positive SST anomalies in the equatorial central and eastern Pacific tend to be weaker. These results suggest that ENSO evolution from the preceding winter to summer experiences a decadal change around the late 1990s, and ENSO-related summer SST anomalies, particularly those in MC, induce interannual variability of CEF through the convection anomalies over MC.

Similar changes of ENSO evolution, especially SST anomalies in MC have also been

mentioned by previous studies (Feng et al., 2014; Song and Zhou, 2015), which indicated that the background of IPO (PDO) phase may modulate the ENSO decaying. They also pointed out that during negative IPO phases, ENSO may decay more rapidly without strong SST anomalies in the Indian Ocean. These changes are also reflected in our results. Therefore, the negative JJA SST anomalies in MC and relatively quick ENSO decaying in the latter period may be attributed to the fact that IPO underwent a transition to the negative phase around the late 1990s (Parker et al. 2007; Henley et al. 2015).

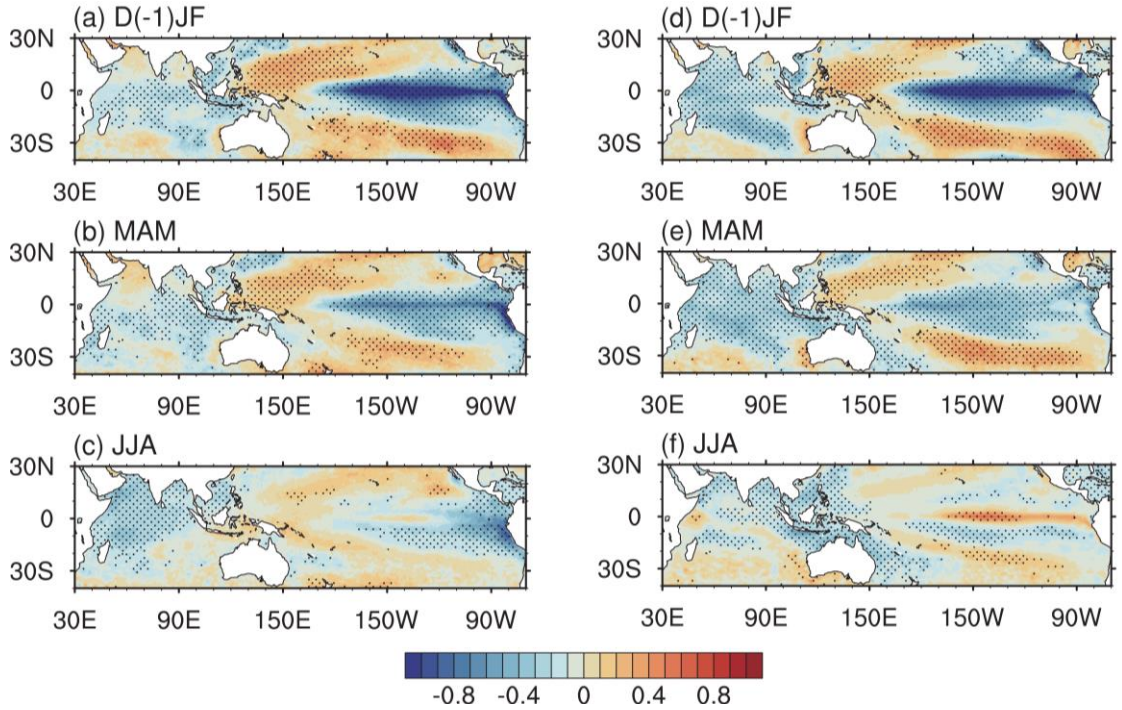

Fig. 11 Regression of the SST (ºC) in (a) D(−1)JF, (b) MAM and (c) JJA onto the Niño 3.4 index in D(–1)JF for the time period of 1979−1997. The red (blue) shading denotes the positive (negative) values, and dots represent regions significant at the 95% confidence level based on the Student's *t*-test. (d−f) are the same as (a−c), but for the time period of 1998−2020.

6 Summary and discussion

The interannual variability of the CEF in the lower troposphere over MC is highly correlated with that in the upper troposphere. In this study, we regarded these two as a whole and investigated the tropical anomalies associated with a combined CEF index. Observational diagnostics show that strengthened CEF is associated with the large-scale circulation anomalies in the tropics, characterized by upper-tropospheric northeasterly anomalies across MC, weakened Walker circulation, and anomalous upper-tropospheric anticyclonic and

lower-tropospheric cyclonic circulation over the tropical WNP. Corresponding convection anomalies to the strengthening of CEF are showing as suppressed convection over MC and enhanced convection over the central Pacific and tropical WNP, consistent well with the above-mentioned circulation anomalies. Besides, strengthened CEF associates with both La Niña-like SST anomalies in the preceding seasons and El Niño-like SST anomalies from the simultaneous summer to the following winter.

We further indicated how the ENSO in both the preceding winter and simultaneous summer can significantly affect CEF variability via tropical convection anomalies using an LBM. Results show that the prescribed heating over WNP and cooling MC in the model can reproduce well the observational circulation anomalies associated with CEF in both upper- and lower-level troposphere, suggesting that the tropical convection plays a crucial role in affecting CEFs. The prescribed heating over WNP triggers the northeasterlies across MC in the upper troposphere and cyclonic circulation over WNP in the lower troposphere, and the cooling over MC induces the weakened Walker circulation. These circulation responses are in good agreement with observational circulation anomalies associated with CEF strengthening.

The stability of the relationships between CEF and SST anomalies in both the preceding winter and simultaneous summer was further examined. Results show that the relationship between CEF and SST anomalies in the preceding winter experiences a decadal change around 1997/98: CEFI is barely correlated with D(−1)JF Niño3.4 index in the former period (−0.08), but is significantly correlated in the latter period (−0.64). This decadal strengthening of the relationship can be attributed to the decadal change of ENSO evolution from the preceding winter to summer around the late 1990s. In the latter period, negative SST anomalies in the equatorial central and eastern Pacific in the preceding winter are followed by negative summer SST anomalies in MC, which can lead to stronger CEF via the suppressed convections over MC. However, summer SST and convection anomalies, associated with the preceding ENSO, are weak over MC in the former period. By contrast to the preceding SST anomalies, the simultaneous summer SST anomalies in the equatorial central and eastern Pacific show a stable and close relationship to CEF.

Although the present study suggests that the anomalous convection over WNP and MC affects the large-scale circulations in the tropics and CEFs, it does not exclude the possibility

that the latter can, in turn, affect the former. It is well known that circulation anomalies can favor and maintain convection in the tropics. Specifically, the westerly anomalies in association with the lower-tropospheric cyclonic anomaly over the WNP may favor the water vapor transport into the region and favor convection over there. Therefore, the relationship between the convection and large-scale circulation anomalies mentioned in this study should be considered as a coupled one.

Previous studies indicated the high prediction skills on the precipitation/convection over WNP and MC (Chowdary et al. 2010; Lee et al. 2011; Li et al. 2012, 2013; Zhang et al. 2016). Would the predictability of CEF be correspondingly high due to the close relationship between CEF and convection anomalies? In addition, the variability in atmospheric convection exhibits a multi-scale feature from diurnal to interdecadal time scales over both WNP and MC (Li and Wang 2005; Hsu et al. 2014; Yoneyama and Zhang 2020). Therefore, it can be expectable that there would be coupling between CEF and convection on different time scales and the multi-scale interactions in association with CEF variability. The predictability and multi-scale features of CEF needs to be further investigated.

Acknowledgments

This research was supported by the National Natural Science Foundation of China (Grant Nos. 41875072, 41721004 and 41705044). B.D. is supported by the U.K. National Centre for Atmospheric Science at the University of Reading.

Data Availability Statement

All data used in this paper are open accessed. The ERA-Interim data are available from ECMWF (https://apps.ecmwf.int/datasets/). GPCP precipitation and the interpolated OLR data are provided by the NOAA/OAR/ESRL PSL, Boulder, Colorado, USA (https://psl.noaa.gov/).

REFERENCES

Adler, R. F., and Coauthors, 2003: The version-2 global precipitation climatology project (GPCP) monthly precipitation analysis (1979–Present). *J. Hydrometeor.*, **4**, 1147–1167.

As-syakur, A. R., and Coauthors, 2014: Observation of spatial patterns on the rainfall response to ENSO and IOD over Indonesia using TRMM Multisatellite Precipitation Analysis (TMPA). *Int. J. Climatol*, **34**, 3825–3839, doi:10.1002/joc.3939.

Chen, W., J.-K. Park, B. Dong, R. Lu, and W.-S. Jung, 2012: The relationship between El Niño and the western North Pacific summer climate in a coupled GCM: Role of the transition of El Niño decaying phases. *J. Geophys. Res.*- Atmospheres, **117**, D12111, doi:10.1029/2011jd017385.

Chowdary, J. S., S.-P. Xie, J.-Y. Lee, Y. Kosaka, and B. Wang, 2010: Predictability of summer northwest Pacific climate in 11 coupled model hindcasts: Local and remote forcing. *J. Geophys. Res.*, **115**, D22121, doi:10.1029/2010jd014595.

Cong, J., Z. Y. Guan, and L. J. Wang, 2007: Interannual (interdecadal) variabilities of two cross-equatorial flows in association with the Asian summer monsoon variations. *J. Nanjing Inst. Meteor. (in Chinese)*, **30**, 779–785.

Dai, A., and T. M. L. Wigley, 2000: Global patterns of ENSO-induced precipitation. *Geophys. Res. Lett.*, **27**, 1283–1286, doi:10.1029/1999gl011140.

Dao, S. Y., S. Y. Hsu, and C. Y. Kuo, 1962: The characteristics of the zonal and meridional circulation over tropical and subtropical regions in Eastern Asia in summer(in Chinese). *Acta Meteor. Sinica* , **32**, 91–103.

Feng, J., L. Wang, and W. Chen, 2014: How Does the East Asian Summer Monsoon Behave in the Decaying Phase of El Niño during Different PDO Phases? *J. Climate*, **27**, 2682–2698, doi: 10.1175/jcli-d-13-00015.1.

Feng, T., X. Y. Shen, R. H. Huang, and G. H. Chen, 2017: Influence of the interannual variation of cross-equatorial flow on tropical cyclogenesis over the western North Pacific. *J. Trop. Meteor*, **23**, 68–80.

Findlater, J., 1969: Interhemispheric transport of air in the lower troposphere over the western Indian Ocean. *Quart. J. Roy. Meteor. Soc.*, **95**, 400–403, doi:10.1002/qj.49709540412.

Fukutomi, Y., C. Kodama, Y. Yamada, A. T. Noda, and M. Satoh, 2015: Tropical synoptic-scale wave disturbances over the western Pacific simulated by a global

574 cloud-system resolving model. *Theor. Appl. Climatol.*, **124**, 737–755,
575 doi:10.1007/s00704-015-1456-4.

576 Gao, H., and F. Xue, 2006: Seasonal variation of the cross-equatorial flows and their
577 influences on the onset of south china sea summer monsoon(in Chinese). *Climatic*
578 *Environ Res*, **11**, 57–68.

579 Held, I. M., S. W. Lyons, and S. Nigam, 1989: Transients and the extratropical response to El
580 Niño. *J. Atmos. Sci.*, **46**, 163–174.

581 Henley BJ, Gergis J, Karoly DJ, Power S, Kennedy J, Folland CK, 2015: A tripole index for
582 the interdecadal Pacific oscillation. *Climate Dyn.*, **45**, 3077–3090.

583 Hersbach Hans, and Coauthors, 2010: The ERA5 global reanalysis. *Quart. J. Roy. Meteor.*
584 *Soc.*, **146**, 1999–2049, doi:10.1002/qj.3803.

585 Hirota, N., and M. Takahashi, 2012: A tripolar pattern as an internal mode of the East Asian
586 summer monsoon. *Climate Dyn.*, **39**, 2219–2238, doi:10.1007/s00382-012-1416-y.

587 Hsu, H.-H., T. Zhou, and J. Matsumoto, 2014: East Asian, Indochina and western North
588 Pacific Summer Monsoon-An update. Asia-Pac *J. Atmos. Sci.*, **50**, 45–68,
589 doi:10.1007/s13143-014-0027-4.

590 Huang, R., and L. Li, 1989: Numerical simulation of the relationship between the anomaly of
591 subtropical high over East Asia and the convective activities in the western tropical
592 Pacific. *Adv. Atmos. Sci.*, **6**, 202–214, doi:10.1007/bf02658016.

593 Kang, I.-S., and J.-S. Kug, 2006: Interactive feedback between ENSO and the Indian Ocean. *J.*
594 *Climate*, **19**, 1784-1801, doi:10.1175/jcli3660.1.

595 Kao, H.-Y., and J.-Y. Yu, 2009: Contrasting eastern-Pacific and central-Pacific types of
596 ENSO. *J. Climate*, **22**, 615–632, doi:10.1175/2008jcli2309.1.

597 Kosaka, Y., and H. Nakamura, 2010: Mechanisms of meridional teleconnection observed
598 between a summer monsoon system and a subtropical anticyclone. Part I: The Pacific–
599 Japan pattern. *J. Climate*, **23**, 5085–5108, doi:10.1175/2010jcli3413.1.

600 Kug, J.-S., F.-F. Jin, and S.-I. An, 2009: Two Types of El Niño Events: Cold Tongue El Niño
601 and Warm Pool El Niño. *J. Climate*, **22**, 1499–1515, doi:10.1175/2008jcli2624.1.

602 Kumar, K. K., B. Rajagopalan, and M. A. Cane, 1999: On the weakening relationship
603 between the Indian monsoon and ENSO. *Science*, **284**, 2156–2159,
604 doi:10.1126/science.284.5423.2156.

605 Lee, S.-S., J.-Y. Lee, K.-J. Ha, B. Wang, and J. K. E. Schemm, 2011: Deficiencies and
606 possibilities for long-lead coupled climate prediction of the western North Pacific-East
607 Asian summer monsoon. *Climate Dyn.*, **36**, 1173–1188, doi:10.1007/s00382-010-0832-0.

608 Li, C., and S. Li, 2014: Interannual seesaw between the Somali and the Australian
609 cross-equatorial flows and its connection to the East Asian summer monsoon. *J. Climate*,
610 **27**, 3966–3981, doi:10.1175/jcli-d-13-00288.1.

611 ——, J.-J. Luo, and S. Li, 2017: Impacts of different types of ENSO on the interannual
612 seesaw between the Somali and the Maritime Continent cross-equatorial flows. *J. Climate*,
613 **30**, 2621-2638, doi:10.1175/jcli-d-16-0521.1.

614 Li, C., R. Lu, and B. Dong, 2012: Predictability of the western North Pacific summer climate
615 demonstrated by the coupled models of ENSEMBLES. *Climate Dyn.*, **39**, 329–346,
616 doi:10.1007/s00382-011-1274-z.

617 ——, 2013: Predictability of the western North Pacific summer climate associated with
618 different ENSO phases by ENSEMBLES multi-model seasonal forecasts. *Climate Dyn.*,
619 **43**, 1829–1845, doi:10.1007/s00382-013-2010-7.

620 Li, S., and Coauthors, 2018: Chemical evidence of inter-hemispheric air mass intrusion into
621 the Northern Hemisphere mid-latitudes. *Sci. Rep.*, **8**, 4669,
622 doi:10.1038/s41598-018-22266-0.

623 Li, T., and B. Wang, 2005: A Review on the western North Pacific monsoon:
624 Synoptic-to-interannual variabilities. *Terr. Atmos. Ocean. Sci.*, **16**, 285–314,
625 doi:10.3319/tao.2005.16.2.285(a).

626 Li, Z. Z., C. H., Qian, and C. R. Sun, 2000: A priliminary analysis on the relationship between
627 the cross-equatorial flow and the heavy rainfall over Yangtze and Huaihe River in 1991
628 (in Chinese). *Acta Meteor. Sinica*, **58**, 628–636.

629 Liebmann, B., and C. A. Smith, 1996: Description of a complete (interpolated) outgoing
630 longwave radiation dataset. *Bull. Amer. Meteor. Soc.*, **77**, 1275–1277.

631 Lin, Y.-W., LinHo, and C. Chou, 2014: The role of the New Guinea cross-equatorial flow in
632 the interannual variability of the western North Pacific summer monsoon. *Environ. Res.*
633 *Lett.*, **9**, 044003.

634 Lu, R., 2001: Interannual variability of the summertime north Pacific subtropical high and its
635 relation to atmospheric convection over the warm pool. *J. Meteor. Soc. Japan*, **79**, 771–
636 783, doi:10.2151/jmsj.79.771.

637 Lu, R., and B. Dong, 2001: Westward extension of north Pacific subtropical high in summer.
638 *J. Meteor. Soc. Japan*, **79**, 1229–1241, doi:10.2151/jmsj.79.1229.

639 Nitta, T., 1987: Convective activities in the tropical western Pacific and their impact on the
640 Northern Hemisphere summer circulation. *J. Meteor. Soc. Japan. Ser. II*, **65**, 373–390,
641 doi:10.2151/jmsj1965.65.3_373.

642 Parker D, Folland C, Scaife A, Knight J, Colman A, Baines P, Dong B, 2007: Decadal to
643 multidecadal variability and the climate change background. *J. Geophys. Res.*, **112**,
644 D18115.

645 Philander, S. G., 1990: El Niño, La Niña, and the Southern Oscillation. Academic Press. New
646 York, 293pp.

647 Rodwell, M. J., and B. J. Hoskins, 1995: A model of the Asian summer monsoon. Part II:
648 Cross-equatorial flow and PV behavior. *J. Atmos. Sci.*, **52**, 1341–1356.

649 Schiemann, R., M. E. Demory, M. S. Mizielinski, M. J. Roberts, L. C. Shaffrey, J. Strachan,
650 and P. L. Vidale, 2014: The sensitivity of the tropical circulation and Maritime Continent
651 precipitation to climate model resolution. *Climate Dyn.*, **42**, 2455–2468,
652 doi:10.1007/s00382-013-1997-0.

653 Schneider, T., Bischoff, T. and Haug, G, 2014: Migrations and dynamics of the intertropical
654 convergence zone. *Nature*, **513**, 45–53.

655 Shi, N., G. L. Feng, J. Q. Gu, D. J. Gu, and J. H. Yu, 2007: Climatological variation of global
656 cross-equatorial flows for the period 1948–2004. *J. Trop. Meteor.* **13**, 201–204.

657 Song, F., L.R. Leung, J. Lu and L. Dong, 2018a: Future changes in seasonality of the North
658 Pacific and North Atlantic subtropical highs, *Geophys. Res. Lett.*, **45**, 11959–11968.

659 ——, ——, ——, and ——, 2018b: Seasonally-dependent responses of subtropical highs
660 and tropical rainfall to anthropogenic warming. *Nature Climate Change*, **8**, 787–792.

——, and T. Zhou, 2014a: The climatology and interannual variability of East Asian summer monsoon in CMIP5 coupled models: Does air–sea coupling improve the simulations? *J. Climate*, **27**, 8761–8777, doi:10.1175/jcli-d-14-00396.1.

——, and ——, 2014b: Interannual variability of East Asian summer monsoon simulated by CMIP3 and CMIP5 AGCMs: Skill dependence on Indian Ocean–western Pacific anticyclone teleconnection. *J. Climate*, **27**, 1679–1697, doi:10.1175/jcli-d-13-00248.1.

——, and ——, 2015: The crucial role of internal variability in modulating the decadal variation of the East Asian summer monsoon–ENSO relationship during the twentieth century. *J. Climate*, **28**, 7093–7107, doi: 10.1175/jcli-d-14-00783.1.

Tang, B., P. W. Guo, and L. P. Yang, 2009: Interannual variaiton of summer cross-equatorial flow in lower troposphere in Eastern Hemisphere. *J. Nanjing Inst. Meteor. (in Chinese)*, **32**, 298–305, doi:10.13878/j.

Wang, B., and Z. Fan, 1999: Choice of South Asian summer monsoon indices. *Bull. Amer. Meteor. Soc.*, **80**, 629–638.

——, R. G. Wu, and T. Li, 2003: Atmosphere-warm ocean interaction and its impacts on Asian-Australian monsoon variation. *J. Climate*, **16**, 1195–1211.

——, ——, and X. H. Fu, 2000: Pacific-East Asian teleconnection: how does ENSO affect East Asian climate? *J. Climate*, **13**, 1517–1536.

Wang, H. J., and F. Xue, 2003: Interannual variability of Somali Jet and its influences on the inter-hemispheric water vapor transport and on the East Asian summer rainfall. *Chinese J. Geophys. (in Chinese)*, **46**, 18–25, doi:10.1002/cjg2.311.

Wang, J. Z., and M. C. Li, 1982: Cross-equator flow from Australia and monsoon over China. *Scientia Atmos. Sinica (in Chinese)*, **6**, 1–10.

Wang, W. P., and X. Q. Yang, 2008: Variation of Somali jet and its impact on East Asian summer monsoon and associated China rainfall anomalies. *Scientia Meteor. Sinica (in Chinese)*, **28**, 139–146.

——, and ——, 2014: Relationship between Somali jet and Australia cross-equatorial flow interannual variabilities and its impact. *J. Meteor. Sci. (in Chinese)*, **34**, 591–600.

689 Watanabe, M., and M. Kimoto, 2000: Atmosphere-ocean thermal coupling in the north
690 Atlantic: A positive feedback. *Quart. J. Roy. Meteor. Soc.*, **126**, 3343–3369,
691 doi:10.1002/qj.49712657017.

692 ——, 2001: Corrigendum. *Quart. J. Roy. Meteor. Soc.*, **127**, 733–734,
693 doi:10.1002/qj.49712757223.

694 ——, and F.-F. Jin, 2004: Dynamical prototype of the Arctic Oscillation as revealed by a
695 neutral singular vector. *J. Climate*, **17**, 2119–2138.

696 Wu, B., T. Zhou, and T. Li, 2009: Seasonally evolving dominant interannual variability
697 modes of East Asian climate. *J. Climate*, **22**, 2992–3005, doi:10.1175/2008jcli2710.1.

698 ——, T. Li, and T. Zhou, 2010: Relative contributions of the Indian Ocean and local SST
699 anomalies to the maintenance of the western North Pacific anomalous anticyclone during
700 the El Niño decaying summer. *J. Climate*, **23**, 2974–2986, doi:10.1175/2010jcli3300.1.

701 Wu, M. M. and L. Wang, 2019: Enhanced correlation between ENSO and western North
702 Pacific monsoon during boreal summer around the 1990s. *Atmos. Oceanic Sci. Lett.*, **12,**
703 **376**–384, doi: 10.1080/16742834.2019.1641397.

704 Wu, R., and B. Wang, 2002: A Contrast of the East Asian summer monsoon–ENSO
705 relationship between 1962–77 and 1978–93. *J. Climate*, **15**, 3266–3279.

706 Xiang, B., B. Wang, and T. Li, 2012: A new paradigm for the predominance of standing
707 Central Pacific Warming after the late 1990s. *Climate Dyn.*, **41**, 327–340,
708 doi:10.1007/s00382-012-1427-8.

709 Xie, S.-P., K. Hu, J. Hafner, H. Tokinaga, Y. Du, G. Huang, and T. Sampe, 2009: Indian
710 Ocean capacitor effect on Indo–Western Pacific climate during the summer following El
711 Niño. *J. Climate*, **22**, 730–747, doi:10.1175/2008jcli2544.1.

712 ——, Y. Kosaka, Y. Du, K. Hu, J. S. Chowdary, and G. Huang, 2016: Indo-western Pacific
713 Ocean capacitor and coherent climate anomalies in post-ENSO summer: A review. *Adv.*
714 *Atmos. Sci.*, **33**, 411–432, doi:10.1007/s00376-015-5192-6.

715 Xu, Y. M., 2011: The genesis of tropical cyclone Bilis (2000) associated with cross-equatorial
716 surges. *Adv Atmos Sci*, **28**, 665–681.

717 Yeh, S. W., J. S. Kug, B. Dewitte, M. H. Kwon, B. P. Kirtman, and F. F. Jin, 2009: El Nino in
718 a changing climate. *Nature*, **462**, 511–514, doi:10.1038/nature08546.

719 ——, X. Wang, C. Wang, and B. Dewitte, 2015: On the relationship between the North
720 Pacific climate variability and the central Pacific El Niño. *J. Climate*, **28**, 663-677,
721 doi:10.1175/jcli-d-14-00137.1.

722 Yoneyama, K., and C. Zhang, 2020: Years of the Maritime Continent. *Geophys. Res. Lett.*, **47**,
723 doi:10.1029/2020gl087182.

724 Yu, J.-Y., M.-M. Lu, and S. T. Kim, 2012: A change in the relationship between tropical
725 central Pacific SST variability and the extratropical atmosphere around 1990. *Environ.*
726 *Res. Lett.*, **7**, doi:10.1088/1748-9326/7/3/034025.

727 Yuan, Y., and S. Yang, 2012: Impacts of different types of El Niño on the East Asian climate:
728 Focus on ENSO Cycles. *J. Climate*, **25**, 7702–7722, doi:10.1175/jcli-d-11-00576.1.

729 Zeng, Q. C., and J. P. Li, 2002: Interactions between the Northern and Southern Hemispheric
730 atmospheres and the essence of monsoon (in Chinese). *Chin. J. Atmos. Sci.*, **26**, 433–448.

731 Zhang, T., S. Yang, X. Jiang, and P. Zhao, 2016: Seasonal–interannual variation and
732 prediction of wet and dry season rainfall over the Maritime Continent: Roles of ENSO and
733 monsoon circulation. *J. Climate*, **29**, 3675–3695, doi:10.1175/jcli-d-15-0222.1.

734 Zhao, H., and C. Wang, 2018: On the relationship between ENSO and tropical cyclones in the
735 western North Pacific during the boreal summer. *Climate Dyn.*, **52**, 275–288,
736 doi:10.1007/s00382-018-4136-0.

737 Zhao, X., and R. Lu, 2020: Vertical structure of interannual variability in cross-equatorial
738 flows over the Maritime Continent and Indian Ocean in boreal summer. *Adv. Atmos. Sci.*,
739 **37**, 173–186, doi:10.1007/s00376-019-9103-0.

740 Zhou, X., R. Lu, G. Chen, and L. Wu, 2018: Interannual variations in synoptic-scale
741 disturbances over the western North Pacific. *Adv. Atmos. Sci.*, **35**, 507–517,
742 doi:10.1007/s00376-017-7143-x.

743 Zhu, Y., 2012: Variations of the summer Somali and Australia cross-equatorial flows and the
744 implications for the Asian summer monsoon. *Adv. Atmos. Sci.*, **29**, 509–518,
745 doi:10.1007/s00376-011-1120-6.

746 Zhuang, M., and A. Duan, 2019: Revisiting the cross-equatorial flows and Asian summer
747 monsoon precipitation associated with the Maritime Continent. *J. Climate*, **32**, 6803–6821,
748 doi:10.1175/jcli-d-18-0749.1.